The use of electron maps to constrain some physical properties of solar flares

A. M. Massone[1] and M. Piana[1,2]

ABSTRACT

The most direct representation of the measurements provided by the *Reuven Ramaty High Energy Solar Spectroscopic Imager (RHESSI)* is a set of Fourier components of the X-ray radiation sampled at discrete points of the spatial frequency plane, the so called visibilities. Here we review methods for the reconstruction of X-ray and electron maps using *RHESSI* visibilities and show how the electron maps can be utilized to infer information on the physical properties of the acceleration region during flaring events.

Subject headings: Sun: flares; sun: x-rays; methods: regularization; methods: positivity constraint

1. Introduction

Astronomical research frequently requires to solve inverse problems of a peculiarly difficult nature. In fact astronomers often find themselves in the uncomfortable role of remote observers attempting to model an unknown source distribution which, by means of unknown processes, emits photons which propagate, via poorly known mechanisms, up to the observing instrument where they become data at disposal only after a final convolution with the (hopefully known) instrument response. With a single statement of a more mathematical flavor, this whole process can be translated as follows: in several cases the interpretation of astronomical observations may be reduced to the inverse problem of processing data which have been subject to an extremely complicated and mostly unknown blurring mechanism, with the aim of reconstructing the physically significant parameters of the source where the radiated information come from.

[1]CNR - Consiglio Nazionale delle Ricerche, SPIN, Genova, via Dodecaneso 33, I-16146 Genova, Italy

[2]Dipartimento di Matematica, Università di Genova, via Dodecaneso 35, I-16146 Genova, Italy

According to a rough classification, two typologies of inverse problems in astronomy can be designed. *Instrumental Problems* consist of the attempt to understand or measure an underlying process after it has been distorted by the instrument utilized to measure it (typical examples are provided by different kinds of image reconstruction problems). *Interpretation Problems* consist of the attempt to understand or measure an underlying process, after it has been transformed by the effects of some other astrophysical phenomenon into observable data.

In the case of the NASA *Reuven Ramaty High Energy Solar Spectroscopic Imager (RHESSI)* mission (Lin et al 2002) the important issue of extracting physically meaningful information from the observed data involves both a tricky instrumental inverse problem and an interpretation inverse problem characterized by a notable numerical instability. In fact, *RHESSI* imaging works by **X-ray flux modulation** rather than by focusing, in a way recalling how interferometric radio telescopes image the sky (Hurford et al 2002). The rotation of the grid pairs of each one of its nine Rotating Modulation Collimators (RMCs) provides a temporal modulation of the incoming X-rays and the pattern of such temporal modulation provides not an image but rather a specific set of spatial Fourier components of the source, called visibilities. These visibilities, which are complex numbers with corresponding complex error bars, are fully calibrated, containing no instrumental dependence other than the instrumentally defined spatial frequencies **and the off-diagonal terms in the Detector Response Matrix**, are not biased by background and, thanks to symmetry properties of the imaging system, offer a level of redundant information that can be exploited as indication of systematic errors. The *RHESSI* image reconstruction problem is therefore the one of determining X-ray maps of the flaring region from sparse sets of observed visibilities. In Section 2 of this paper a more detailed description of *RHESSI* X-ray visibilities will be given while in Section 3 we will review the basic properties of the X-ray image reconstruction methods **that can be used to solve the *RHESSI* instrumental inverse problem.**

From a physical viewpoint, it is well-established (Brown, 1971; Brown and Emslie, 1988; Brown, Emslie and Kontar, 2003) that X-ray emission is the bremsstrahlung radiation signature of the phase space distribution of electrons in the plasma and that this electron distribution is the information of central interest in the study of solar flares. In spatially unresolved spectroscopy, information retrieval on the electron distribution on the source from *RHESSI* data can be realized by means of traditional forward-fitting techniques or applying regularization techniques for the reduction of noise amplification (Craig and Brown, 1986; Piana, 1994; Brown et al., 2006). In particular, reliable reconstructions of the mean source electron distribution from *RHESSI* hard Xray spectra have been obtained by means of classical zero order and first

order Tikhonov approaches (Piana et al., 2003; Massone et al., 2004; Kontar et al., 2005) and a heuristic technique realizing a triangular matrix row elimination with energy binning (Johns and Lin, 1992). However, in order to physically constrain theoretical models of the acceleration mechanisms in solar plasma during flares, it is much more useful (and much more challenging) to infer information on the spatial distribution of the electron flux spectra at many different electron energies. **In the present paper we will review a computational method for the solution of this significant interpretation inverse problem in the *RHESSI* framework. Specifically, in Section 4 we will describe** a technique that permits to synthesize, at different electron energies, maps of the event whose pixel content is related to the averaged electron flux *in situ*. In Section 5 this method will be applied to one event related to compact sources and the results briefly discussed in the context of simple models of acceleration mechanisms. Finally Section 6 will describe some open problems.

2. *RHESSI* visibilities

RHESSI imaging system is characterized by a rather simple geometry: nine high- sensitivity Germanium detectors are utilized to detect the photons coming from the Sun; each detector is associated with a pair of co-axial collimators; each collimator is made of a planar array of equally-spaced X-ray-opaque slats separated by transparent slits; the nine pairs of grids are characterized by nine different **grid pitches;** finally, the overall system rotates with a rotation period of 4 seconds and, furthermore, the satellite rotates around the Earth at an orbit of around 600 km. *RHESSI* raw data are light curves, i.e. photon-induced counts recorded while the collimators rotate. A technical procedure made of a data stacking step followed by a fitting step transforms these raw data into a set of observable numbers, named visibilities, that represent the **most direct** way with which *RHESSI* may provide its measurements. *RHESSI* visibilities are complex numbers representing measurements of single Fourier components of the source distribution measured at specific spatial frequencies, energy ranges and time ranges. If (u, v) represents a point in the spatial frequency plane and ϵ is a specific photon energy (or, more typically, an energy channel spanning a specific energy bin), the corresponding measured visibility $V(u, v; \epsilon)$ is related to the photon flux $I(x, y; \epsilon)$ emitted from the point (x, y) of the imaging plane by

$$V(u, v; \epsilon) = \int_{-\infty}^{+\infty} dx \int_{-\infty}^{+\infty} dy I(x, y; \epsilon) e^{2\pi i(ux+vy)}, \tag{1}$$

where the values of the frequency pairs (u, v) sampled during the observation are determined by *RHESSI* hardware. Specifically, since the grid pitches of the collimators are arranged in a geometric progression with factor $\sqrt{3}$, the collimators sample the (u, v) plane over circles

with radii $R_i,\ i = 1, \ldots, 9$ distributed according to the same geometric progression from $R_1 = 0.221$ arcsec^{-1} to $R_9 = 0.0027$ arcsec^{-1}.

3. *RHESSI* imaging concept

From an imaging perspective, the main consequence of the definition of visibility is that visibility-based image reconstruction methods in the *RHESSI* framework must implement a Fourier Transform inversion from limited data. In this section we will describe three algorithms realizing this procedure and point out their advantages and drawbacks.

3.1. Visibility Forward Fit

This is a very fast algorithm that involves forward fitting a parameterized geometrical form to the experimental visibilities. This approach is quite effective when the source has a relatively simple structure: Solar SoftWare (SSW) utilizes four possible forms of source structure, i.e. a circular Gaussian function, **a pair of Gaussian functions**, an elliptical Gaussian function and a curved elliptical Gaussian function mimicking a loop. In the case of more complex morphologies the forward-fit reconstruction accuracy rapidly deteriorates and the method becomes highly unreliable.

3.2. Maximum Entropy (MEM)

MEM implements a statistical regularization method where the functional

$$J = H - \alpha\chi^2, \tag{2}$$

$$H = -\sum_{j}^{n_{pix}} \frac{I_j}{I_T} \log\left(\frac{I_j}{I_T}\right), \tag{3}$$

$$I_T = \sum_{j}^{n_{pix}} I_j, \tag{4}$$

$$\chi^2 = \sum_{l=1}^{n_{vis}} \frac{|V_l - V_l'|}{\sigma_l^2} \tag{5}$$

is solved by means of an iterative scheme. In these equations, I is the X-ray image made of n_{pix}, $I_T = \sum_j^{n_{pix}} I_j$ is the total flux in the image I, V is the set of experimental visibilities, V' is the set of visibilities predicted by the image under reconstruction and σ_l, for

$l = 1, \ldots, n_{vis}$, denotes the l-th standard deviation associated to the l-th visibility. The regularization parameter α is obtained by means of optimization techniques. The MEM algorithm implemented in SSW (Bong et al. 2006) provides reliable reconstructions in the case of compact events, although the method often super-resolves the sources and may present convergence problems.

3.3. uv_smooth

This two-step reconstruction algorithm implements an interpolation/extrapolation approach to *RHESSI* image reconstruction (Massone et al 2009). In the first step a visibility surface is created by interpolating the observed visibilities both along the sampling circles and across the spaces between adjacent circles. Specifically, in the routine implemented in SSW, this interpolation step is realized by means of a thin-plate spline interpolation algorithm (Wahba 1990). Then, the problem of reconstructing an X-ray image from the knowledge of experimental and interpolated visibilities uniformly sampling a disk of radius R_1, is accomplished by means of an iterative projected scheme, namely the projected Landweber method (Piana and Bertero 1997). This algorithm implements an inverse Fourier transform method where **at each iteration the reconstructed image is modified by setting to zero all the pixels with negative value. It has been showed (Youla and Webb 1982) that this procedure corresponds to extrapolate reliable Fourier components at spatial frequencies higher than the ones involved by experimental visibilities.** This is a Fast Fourier Transform based scheme and therefore it is very rapid; furthermore it is extremely accurate in the reconstruction of source constellations involving rather limited portions of the field of view. However, updated version of the method are in progress, that reduce possible artifacts showing up when the source configuration is characterized by distant footpoints.

4. Inverse methods and imaging spectroscopy

The physical process that relates hard X-ray emission to the parent distribution of energetic electrons in solar flare plasmas is optically thin electron-ion bremsstrahlung (Brown 1971). The observational parameter is the energy ϵ of the emitted photon; the observed values are the photon flux per unit (two-dimensional) area of the image on the plane of the sky; and the sought-after source function is the spectrum of the energetic electrons, as a function of both position within the source and the source variable E, the electron energy.

Let (x, y) be a point in the image plane containing the source and z be the distance along the line-of-sight into the source at point (x, y). Since the source is optically thin, the relation between the photon spectrum $g(x, y; \epsilon)$ (photons cm^{-2} s^{-1} keV^{-1} arcsec^{-2}) emitted at energy ϵ (keV) from the point (x, y), and the differential electron flux spectrum $F(x, y, z; E)$ (electrons cm^{-2} s^{-1} keV^{-1}) at the point (x, y, z) and at electron energy E (keV) is given by

$$g(x, y; \epsilon) = \frac{a^2}{4\pi R^2} \int_{\epsilon}^{\infty} \int_{0}^{\ell(x,y)} n(x, y, z)\, F(x, y, z; E)\, Q(\epsilon, E)\, dz\, dE \quad , \tag{6}$$

where $R = 1$ AU ($= 1.5 \times 10^{13}$ cm), $a \equiv 7.25 \times 10^7$ cm arcsec^{-1} is the conversion factor from angle subtended at the Earth to distance on the solar surface (so that $R/a = 206265$ arcseconds [$= 1$ radian]) , $\ell(x, y)$ is the line-of-sight depth; $n(x, y, z)$ (cm^{-3}) is the local plasma density; and $Q(\epsilon, E)$ (cm^2 keV^{-1}) is the bremsstrahlung cross-section, differential in photon energy ϵ, representing the probability that a photon of energy ϵ is emitted by an electron of energy E. Equation (6) can be simplified by introducing the *column density* $N(x, y)$ (cm^{-2}) at each point (x, y):

$$N(x, y) = \int_{0}^{\ell(x,y)} n(x, y, z)\, dz \tag{7}$$

and the definition of the *mean electron flux spectrum*

$$\overline{F}(x, y; E) = \frac{1}{N(x, y)} \int_{0}^{\ell(x,y)} n(x, y, z) F(x, y, z; E)\, dz \quad . \tag{8}$$

In fact, using equation (8), (6) may be written

$$g(x, y; \epsilon) = \frac{1}{4\pi R^2} \int_{\epsilon}^{\infty} [a^2\, N(x, y)\, \overline{F}(x, y; E)]\, Q(\epsilon, E)\, dE \quad . \tag{9}$$

This can be further simplified by defining

$$f(x, y; E) := \frac{1}{4\pi R^2}\, [a^2\, N(x, y)\, \overline{F}(x, y; E)] \tag{10}$$

so that

$$g(x, y; \epsilon) = \int_{\epsilon}^{\infty} f(x, y; E)\, Q(\epsilon, E)\, dE \ . \tag{11}$$

In (9)-(11), $f(x, y; E)$ is the source function at different values of the source variable E, $g(x, y; \epsilon)$ is the observed image at different values of the observational parameter ϵ, and

$Q(\epsilon, E)$ quantifies the physical process relating the source function (mean electron flux spectrum) and observed spectrum (photon spectrum). Analytical formulas for $Q(\epsilon, E)$ are available, accounting for all pertinent physics, including relativistic effects, Coulomb screening and electron-electron emission (Koch and Motz 1959).

We now review a general visibility-based imaging spectroscopy procedure for the reconstruction of spatial maps $f(\cdot; E)$ of the source function, at specified values of the source variable E (Piana et al 2007). This method relies on the mathematical fact that the integral relation between the source function $f(x, y; E)$ and the spatially resolved photon spectrum $g(x, y; \epsilon)$ for a fixed (x, y) point (i.e., the bremsstrahlung equation) commutes with the integral relation between the spatially resolved photon spectrum $g(x, y; \epsilon)$ and the observed visibilities $V(u, v; \epsilon)$ at a fixed photon energy ϵ (i.e., the Fourier transform). Therefore we define the electron flux visibility spectrum

$$W(u, v; E) = \int_{-\infty}^{\infty} dx \int_{-\infty}^{\infty} dy f(x, y; E) e^{-2\pi i(ux+vy)} \tag{12}$$

and easily find that the photon flux visibility spectrum and this electron flux visibility spectrum are related by the visibility bremsstrahlung equation

$$V(u, v; \epsilon) = \int_{0}^{\infty} dE Q(\epsilon, E) W(u, v; E). \tag{13}$$

Definition (12) and equation (13) immediately inspire the following reconstruction algorithm:

1. for each (u, v) point sampled by *RHESSI* observation of a given event, solve a discretized version of equation (13) by means of Tikhonov regularization algorithm (Tikhonov et al 1995). This step provides an electron visibility spectrum regularized along the energy direction;

2. for each E value, apply a Fourier-based image reconstruction method (by instance, visibility forward-fit, or maximum entropy, or uv-smooth) to $W(u, v; E)$ in order to obtain an electron map at that energy E. This step provides a set of electron flux maps at many different electron energies.

We point out that the version of the method described in (Piana et al 2007) explicitly accounted for the presence of non-zero off-diagonal elements in the Detector Response Matrix (DRM). However, the error introduced by neglecting this effect is very small and, in any case, the overall imaging spectroscopy scheme still holds (the non-diagonal DRM effects can be encoded in the integral kernel in (13) with no substantial change in the formalism).

This imaging-spectroscopy method has many significant advantages. It utilizes, as input data, photon visibilities, which are the **most direct** form of data provided by *RHESSI*; it implements a smoothing constraint along the electron energy direction, which is physically sound; it is computationally fast, since the number of spectral inversions required (and these are the heaviest steps) is small, corresponding to the number of available visibilities; and, finally, the reconstruction of the electron maps from the electron visibilities can be performed by means of the same Fourier-based imaging algorithms already implemented in the case of X-ray imaging.

5. Electron maps of compact sources

The regularization method described in the previous section has been applied to reconstruct the electron maps of a real event by means of *RHESSI* visibilities. Figure 1 shows X-ray images obtained by means of the maximum entropy method described in Subsection 3.2, while Figure 2 shows electron maps for the same event (and again maximum entropy is used to create the maps from the electron visibilities). For both sets of images, we have represented just the information contained in rectangular boxes where, particularly at low energies (from 10 to 22 keV for the photon maps and from 14 to 42 keV for the electron maps) two footpoints and a coronal source are clearly visible. However, the morphological variations in the set of electron maps are notably smoother with energy than in the case of the photon images, and this is the most direct consequence of a regularization approach in the electron energy direction. Further, the electron maps carry information on the physics at energies much higher than the ones involved by the photon images and this reflects the intrinsic 'rectangularity' of the bremsstrahlung problem. As pointed out in (Piana et al 2003) and (Kontar et al 2004), information on the electron spectrum at high energies is already contained in the photon spectrum at lower energies and can be extracted by means of regularization techniques.

An example of the actual power of this electron-based approach to *RHESSI* imaging spectroscopy is demonstrated in Figure 3, showing the local electron flux spectra directly extracted from the regions (having the same area) in the electron map highlighted by the rectangular boxes. In particular, the electron flux corresponding to the two footpoints have more or less the same intensity at low energies ($E \leq 14$ keV); at intermediate energies ($14 \leq E \leq 30$ keV) the flux spectrum of the northern footpoint becomes a little bit harder while at higher energies the two spectral indices are more or less the same. The flux associated to the middle source is much more intense at low energies but becomes softer very soon and roughly equal to the fluxes of the northern and southern footpoints at around 22 keV and

40 keV, respectively.

This whole picture nicely (and more quantitatively) confirms the physics implicit in the morphologies of the different maps, i.e. the presence of an acceleration region for electrons midway between the two footpoints. This behavior surprisingly agrees with the one obtained with the same technique in the case of the 2002 February 20 event, as described in (Piana et al 2007).

6. Open problems

What we showed in the previous section is a very simple example of how the images of the averaged electron flux at different electron energies can be utilized in order to infer very basic properties of the acceleration region during solar flares. However, many other open issues can be addressed by means of this computational tools. Specifically:

- estimate of the size of the sources can be computed as a function of energy in both the photon and the electron domain in order to predict the mechanism with which the electrons are injected into the emitting region (Xu, Emslie and Hurford 2008);
- determination of the gradient of the electron energies within the coronal loop by solving a continuity equation;
- derivation of parameters like the energy variation of escape and scattering times that constrain the characteristics of stochastic acceleration models (Petrosian and Chen 2010).

These applications can focus on specific events characterized by interesting morphologies or can be utilized in a statistical analysis of lots of events, possibly combining the constraints on the models derived by means of this kind of images with the ones based on observations at other wavelengths. Furthermore, although this approach has been described in the framework of rotating modulation collimators for X-ray imaging, at least in principle it can be applied to all cases where visibilities are involved. A possible example is the analysis of data provided by a multi-element radio interferometer, although in this case a major difficulty is represented by the fact that even the sampling coverage is itself frequency-dependent and therefore a 'gridding' procedure is necessary in the pre-processing stage.

From a computational viewpoint, the main improvements may concern both the inversion method for the spectroscopic step and the reconstruction method for the imaging step. Specifically, we have in mind to introduce spectroscopy algorithms that account for the

statistical properties of the noise on the visibilities and imaging algorithms that explicitly exploit information on the sparsity of the signal.

REFERENCES

Bong, S. C., Lee, J., Gary, D. E. and Yun, H. S. 2006, *Astrophys. J.*, 636, 1159.

Brown, J. C. 1971, *Solar. Phys.*, **18**, 489.

Brown, J. C. and Emslie, A. G. 1988, *Astrophys. J.*, **331**, 554.

Brown, J. C., Emslie, A. G. and Kontar, E. P. 2003, *Astrophys. J.*, **595**, L115.

Brown, J. C. et al 2006, *Astrophys. J.*, 643, 523.

Craig, I. J. D. and Brown, J. C. 1986, *Inverse Problems in Astronomy*, Adam Hilger, New York.

Hurford, G. J. et al. 2002, *Solar Phys.*, **210**, 61.

Johns, C. M. and Lin, R. P. 1992, *Solar Phys.*, **137**, 121.

Koch, H. W. and Motz, J. W. 1959, *Rev. Mod. Phys.* **31**, 920.

Kontar, E. P., Piana, M. Massone, A. M., Emslie, A. G., and Brown, J. C. 2004, *Solar Phys.*, **225**, 293.

Kontar, E. P., Emslie, A. G.; Piana, M., Massone, A. M., and Brown, J. C. 2005, *Solar Phys.*, **226**, 317.

Lin, R. P. et al. 2002, *Solar Phys.*, **210**, 3.

Massone, A. M., Piana, M., Conway, A. J. and Eves, B. 2003, *Astron. Astrophys.*, **405**, 325.

Massone, A. M. et al 2009, *Astrophys. J.*, **703**, 2004.

Petrosian V. and Qingrong, C. 2010, *Astrophys. J.*, **712**, L131.

Piana, M. 1994, *Astron. Astrophys.*, **288**, 949.

Piana, M. and Bertero, M. 1997, *Inverse Problems*, **13**, 441.

Piana, M., Massone, A. M., Kontar, E. P., Emslie, A. G., Brown, J. C., and Schwartz, R. A. 2003, *Astrophys. J.*, **595**, L127.

Tikhonov et al. 1995, Numerical Methods for the Solution of Ill-Posed Problems (Dordrecht: Kluwer).

Wahba, G. 1990, Spline Models for Observational Data (Philadelphia, PA: SIAM)

Xu, Y., Gordon, A. G. and Hurford, G. J. 2008, *Astrophys. J.*, **673**, 576.

Youla, D. C. and Webb, H. 1982 IEEE *Trans. Med. Im.*, 2, 81.

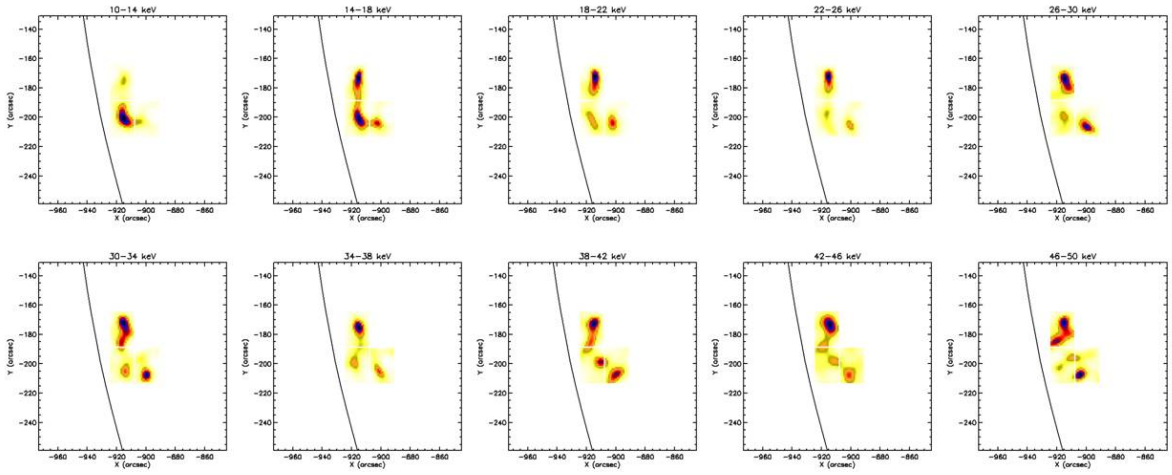

Fig. 1.— Photon maps for the 2002 September 8 (01:38:44 - 01:39:35 UT) event in ten different energy channels from10 keV to 50 keV.

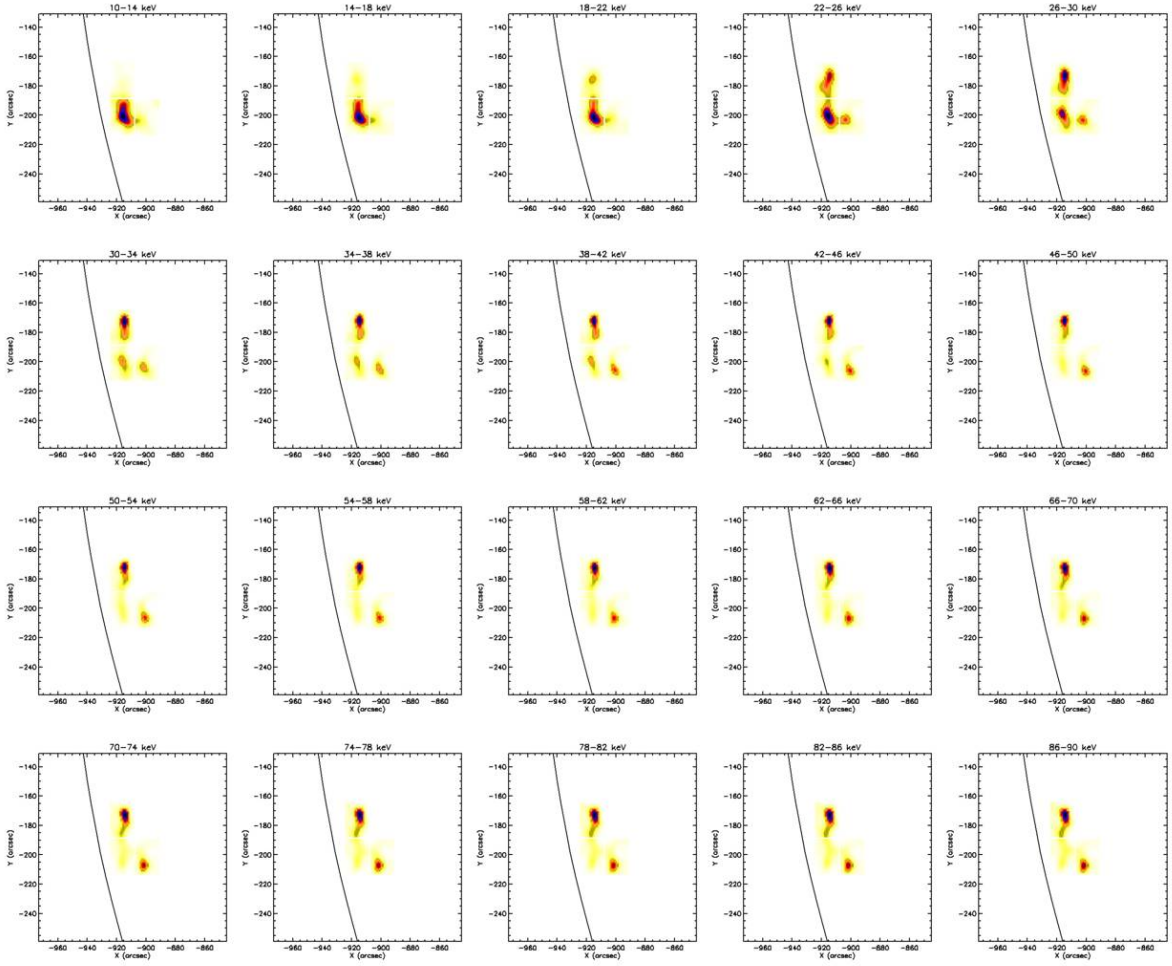

Fig. 2.— Regularized electron maps for the 2002 September 8 (01:38:44 - 01:39:35 UT) event in twenty different energy channels from10 keV to 90 keV.

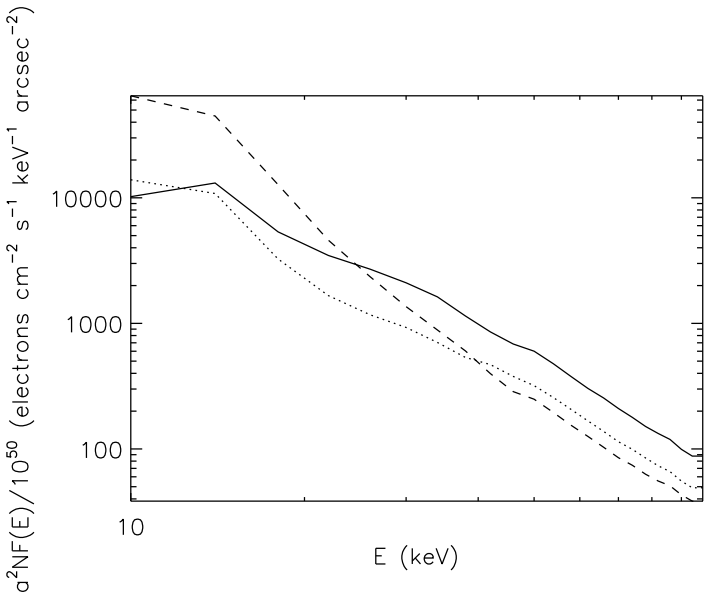

Fig. 3.— Solid: northern footpoint region. Dotted: southern footpoint region. Dashed: intermediate region.